Electronic Supplementary Information (ESI)

The main peak-fitting parameters for the XPS spectra

For all the XPS data collected from samples not sputter cleaned prior to the analysis, the peak-fitting of C1s spectra was performed using the following strategy. A single peak (Gaussian (70%)–Lorentzian (30%)), ascribed to alkyl type carbon (C–C, C–H), is fitted to the main peak of the C 1s spectrum for adventitious carbon. A second peak is usually added that is constrained to be 1.5 eV above the main peak and of equal FWHM to the main peak. This higher BE peak is ascribed to alcohol (C–OH) and/or ester (C–O–C) functionality. Further high BE components (e.g. C=O, 2.8–3.0 eV above the main peak, O–C=O, 3.6–4.3 eV above the main peak) can also be added if required. Spectra from all the samples have been charge corrected to give the adventitious C 1s spectral component (C–C, C–H) a BE of 285.0 eV. The process has an associated error of ±0.1–0.2 eV. As an example, Figure 1 shows the narrow-scan C 1s spectrum recorded on the surface of the as reanodized alumina-free specimen. Thus, three single peaks centered at 285.0 eV for C-H (C-C), 286.6 eV for C-O-C and 288.9 eV for O-C=O species are used to resolve the C 1s spectrum, with the peak-fitting parameters shown in Table 1. After the first 2 sputter cycles, all these peaks almost disappeared from the C 1s spectra. Similar behavior of the C 1s spectrum was revealed for the vacuum-annealed alumina-free sample (not shown) although the surface concentration of C-O-C and O-C=O species was relatively smaller. This confirms that the carbon-containing species are only present in the outermost layer of organic contamination and are not incorporated in the column material.

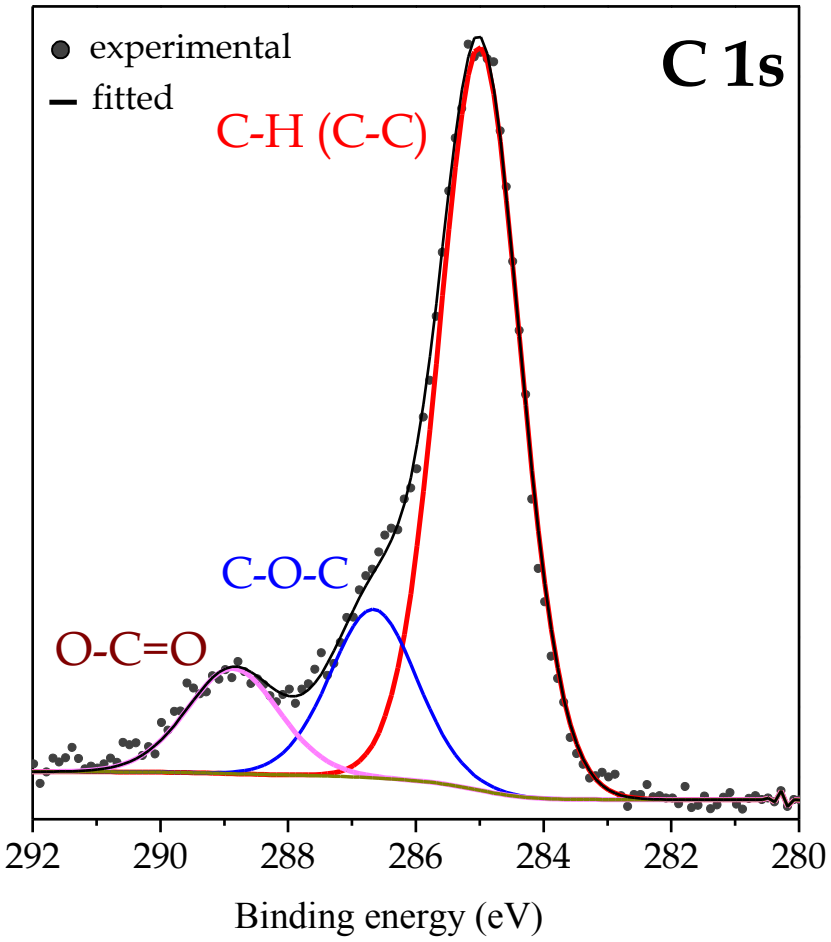

Fig. S1. Experimental and curve-fitted C 1*s* spectrum recorded on the surface of the as reanodized alumina-free specimen (derived from an Al/Nb bilayer anodized at 52 V in 0.2 mol dm^{-3} $H_2C_2O_4$ and then reanodized in 0.1 mol dm^{-3} H_3PO_4 to 300 V)

Table S1. The main peak-fitting parameters for C 1s spectrum components of nanostructured niobium oxide sample derived from Al/Nb layers anodized at 52V in 0.2 mol dm^{-3} $H_2C_2O_4$ and then reanodized in 0.1 mol dm^{-3} H_3PO_4 to 300V

sample	C 1s (eV)	FWHM (eV)	conc. (%)	chemical bond
alumina-free	285.0	1.5	71.3	C-H (C-C)
	286.6	1.5	17.3	C-O-C
	288.9	1.7	11.4	O-C=O

Table S2. The main peak-fitting parameters for Nb 3d spectrum components of the unsputtered surfaces of niobium oxide samples derived from Al/Nb layers anodized at 52V in 0.2 mol dm^{-3} $H_2C_2O_4$ and then reanodized in 0.1 mol dm^{-3} H_3PO_4 to 300V.

sample	Nb $3d_{5/2}$ (eV)	Nb $3d_{3/2}$ (eV)	FWHM (eV)	conc. (%)	compound
alumina-free sample	207.30	210.05	1.13	98.0	Nb_2O_5
	205.65	208.40	1.20	2.0	NbO_2
pore free sample	207.20	209.95	1.07	100.0	Nb_2O_5
vacuum-annealed alumina-free	207.35	210.1	1.10	90.5	Nb_2O_5
	203.85	206.60	1.25	5.8	NbO_2
	205.50	208.25	1.25	3.7	NbO

Table S3. The main peak-fitting parameters for O 1s spectrum components of nanostructured niobium oxide sample derived from Al/Nb layers anodized at 52V in 0.2 mol dm^{-3} $H_2C_2O_4$ and then reanodized in 0.1 mol dm^{-3} H_3PO_4 to 300V.

sample	O 1s (eV)	FWHM (eV)	conc. (%)	chemical bond
as reanodized alumina-free (unetched) sample	533.5	1.3	5.1	H_2O
	532.4	1.3	15.6	OH
	531.6	1.3	29.6	Al-O
	530.5	1.3	49.7	Nb-O
as reanodized alumina-free Ar-ion etched sample	532.8	1.5	5.8	OH
	531.5	1.3	19.0	Al-O
	530.7	1.2	75.2	Nb-O

Details of EDX point analysis of the FIB-made lamella

Prior to sectioning by FIB, a layer of platinum, about 300 nm thick, was deposited over the sample surface for preventing top-surface damage. For TEM observations the sample sections were collected on a copper grid. This explains why there are peaks of Pt and Cu in some of the EDX spectra shown below.

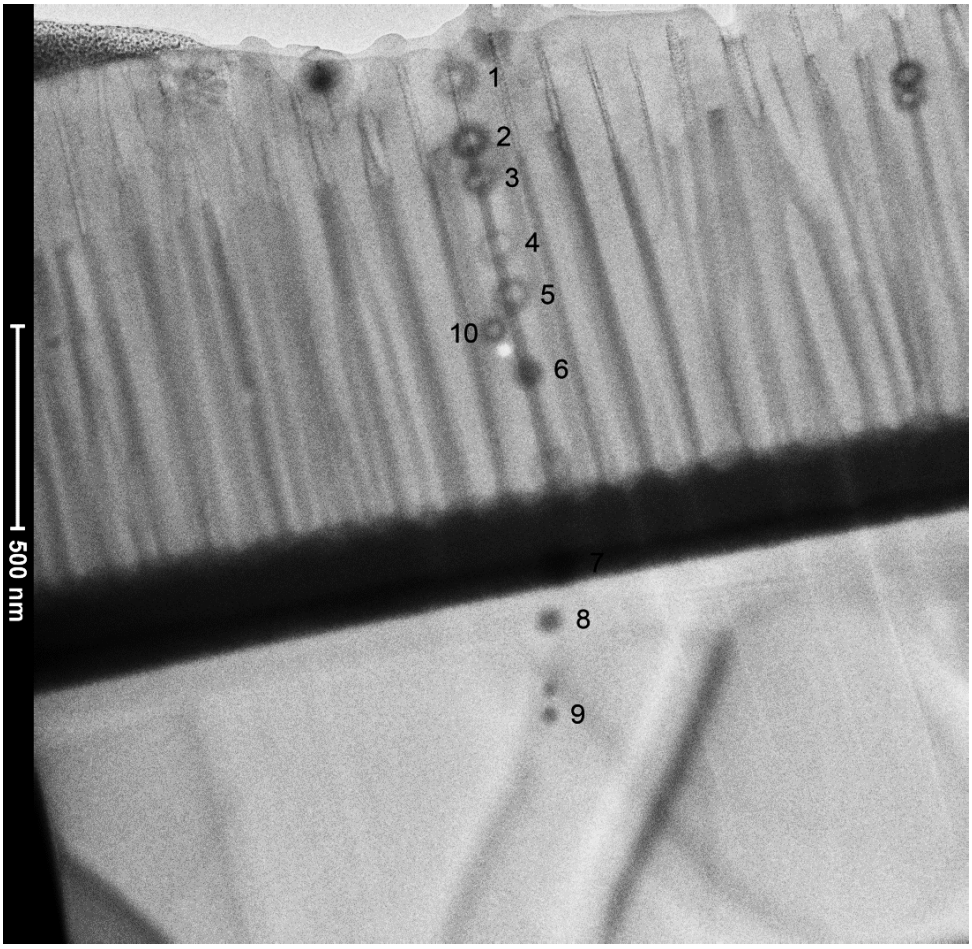

Fig. S2. TEM image of FIB-made lamella of a sample derived from Al/Nb layers on an oxide-coated Al foil anodized at 52 V in 0.2 mol dm^{-3} $H_2C_2O_4$ and then reanodized to 450 V in 0.1 mol dm^{-3} H_3PO_4 soluton (referred to in the main text as the reanodized sample). The spots labelled with digits are the areas of interaction of the electron beam with the sample during the EDX point analysis.

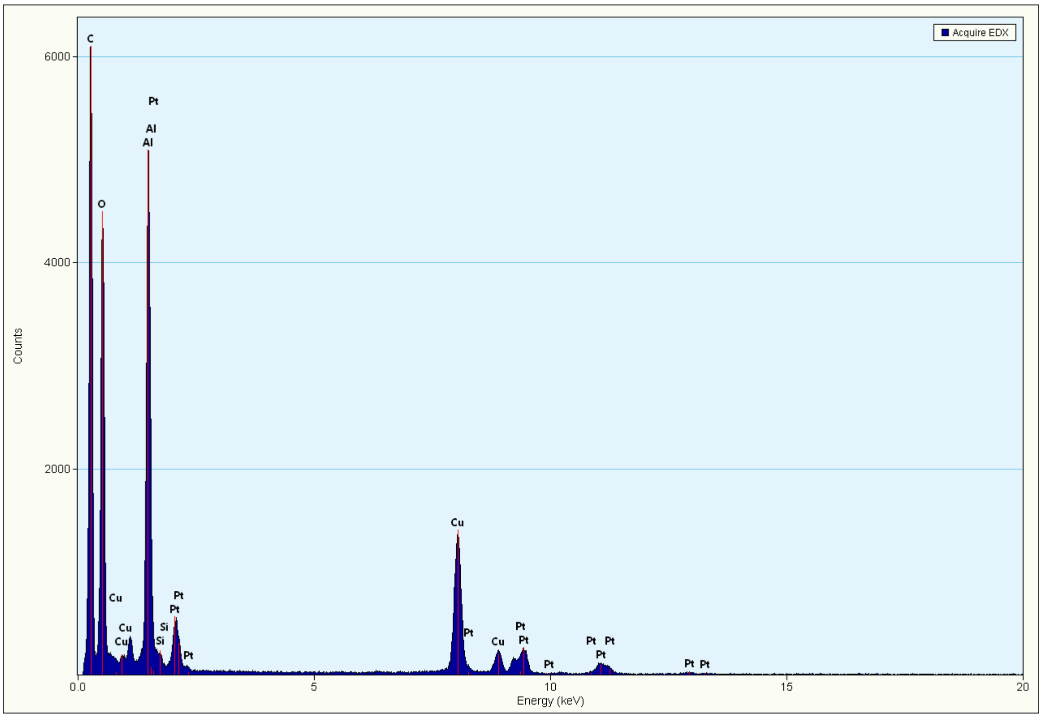

Acquire EDX
Counts
6000
4000
2000
C
O
Pt
Al
Al
Cu
Cu
Cu
Si
Si
Pt
Pt
Pt
Cu
Pt
Cu
Pt
Pt
Pt
Pt
Pt
Pt
Pt
Pt
0.0
5
10
15
20
Energy (keV)

a

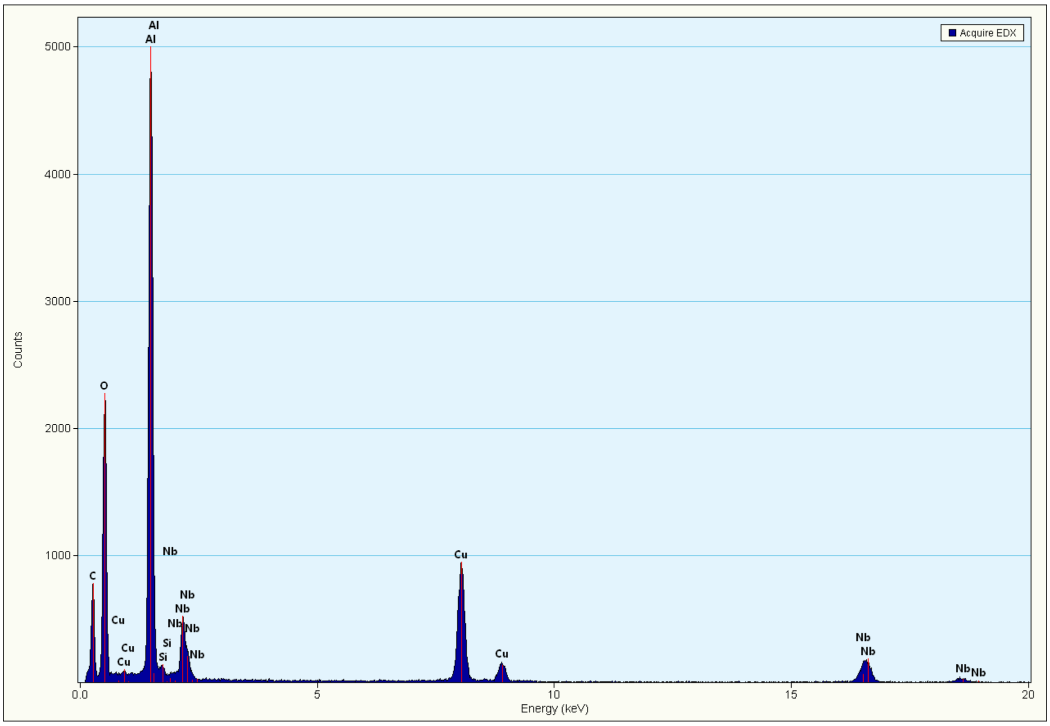

Acquire EDX
Counts
5000
4000
3000
2000
1000
Al
Al
O
C
Cu
Cu
Cu
Nb
Nb
Nb
Nb
Nb
Nb
Si
Si
Cu
Cu
Nb
Nb
Nb
Nb
0.0
5
10
15
20
Energy (keV)

b

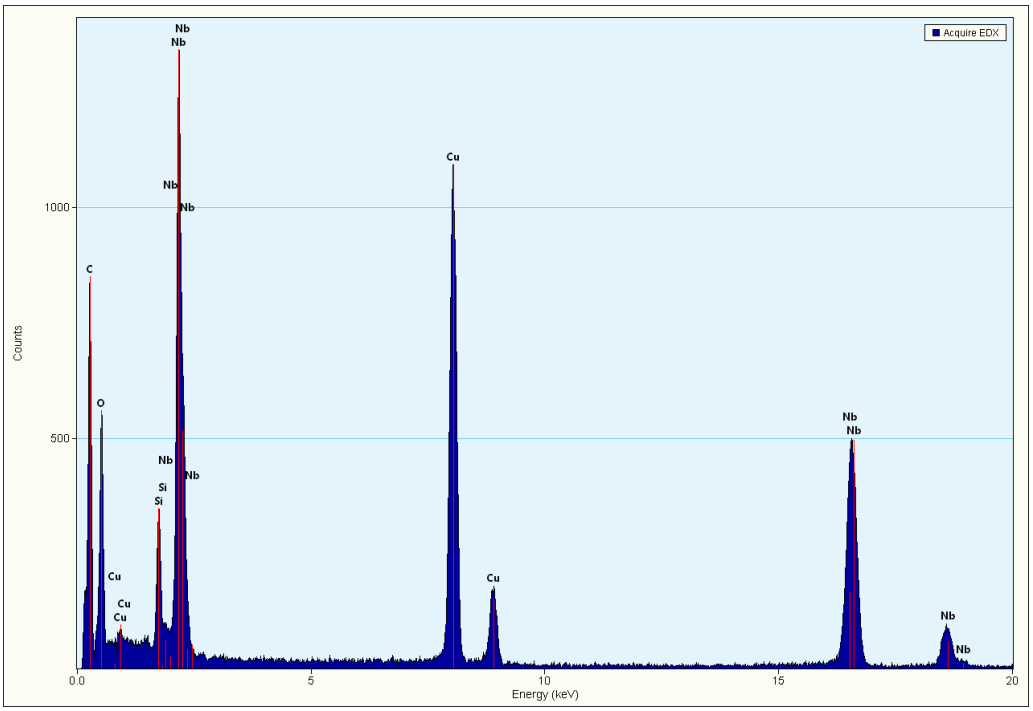

c

Fig. S3. X-ray spectra recorded in (a) spot 1, (b) spot 6, and (c) spot 7 within the FIB-made lamella shown in **Figure S2**.

Details of EDX point analysis of the ultramicrotomed film sections

Ultramicrotomed sections of the anodized Al/Nb bilayers formed on the oxide-coated aluminium foils were prepared using a Reichert-Nissei Ultracuts/FCS ultramicrotom. Fragments of the anodized specimens, encapsulated individually in an epoxy resin, were trimmed initially with a glass knife and suitably thin sections, about 30 nm thick, were prepared by sectioning in a direction approximately parallel to the metal-oxide interface with a diamond knife. Ultramicrotomed sections, collected onto copper grids, were examined in a JEOL JEM-2000FX transmission electron microscope with EDX facilities**.**

Position B (spot size ~5 nm)

Spot				
1	Nb	76.29	at%	$Nb_1O_{0.271136}$
	Al	1.21	at%	Al_2O_3
	O	22.50	at%	
2	Nb	30.31	at%	$Nb_1O_{2.159023}$
	Al	1.70	at%	Al_2O_3
	O	67.99	at%	
3	Nb	23.91	at%	$Nb_1O_{2.596821}$
	Al	5.60	at%	Al_2O_3
	O	70.49	at%	
4	Nb	10.80	at%	$Nb_1O_{4.93287}$
	Al	14.37	at%	Al_2O_3
	O	74.83	at%	
5	Nb	13.42	at%	$Nb_1O_{3.687779}$
	Al	14.84	at%	Al_2O_3
	O	71.75	at%	
6	Nb	13.82	at%	$Nb_1O_{3.343343}$
	Al	15.99	at%	Al_2O_3
	O	70.19	at%	

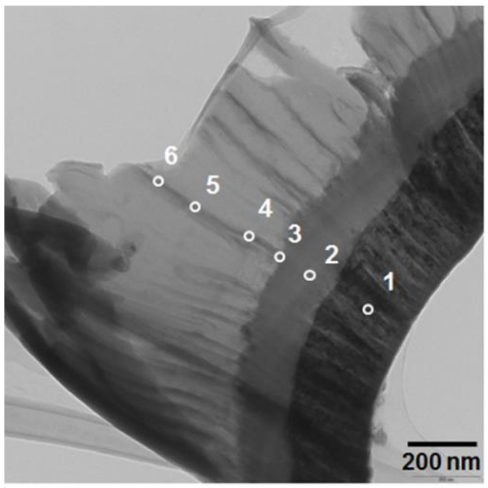

Position A (spot size ~5 nm)

Spot				
1	Nb	79.30	at%	$Nb_1O_{0.188083}$
	Al	2.31	at%	Al_2O_3
	O	18.38	at%	
2	Nb	38.92	at%	$Nb_1O_{1.403006}$
	Al	2.59	at%	Al_2O_3
	O	58.49	at%	
3	Nb	22.22	at%	$Nb_1O_{2.317507}$
	Al	10.51	at%	Al_2O_3
	O	67.26	at%	
4	Nb	4.67	at%	$Nb_1O_{7.704497}$
	Al	23.74	at%	Al_2O_3
	O	71.59	at%	
5	Nb	4.75	at%	$Nb_1O_{6.929474}$
	Al	24.93	at%	Al_2O_3
	O	70.31	at%	
6	Nb	1.72	at%	$Nb_1O_{18.11337}$
	Al	26.85	at%	Al_2O_3
	O	71.43	at%	

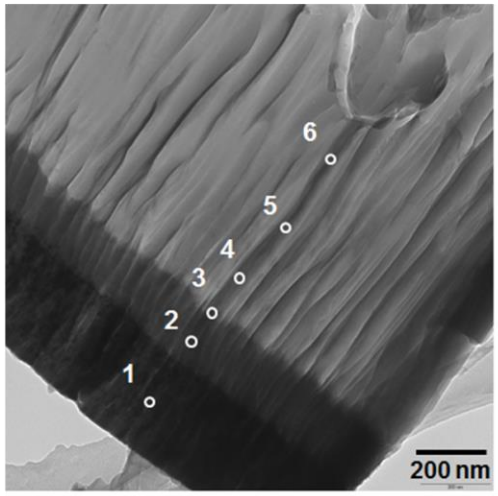

Position C (spot size ~5 nm)

Spot				
1	Nb	81.41	at%	$Nb_1O_{0.214224}$
	Al	0.46	at%	Al_2O_3
	O	18.13	at%	
2	Nb	25.33	at%	$Nb_1O_{2.881767}$
	Al	0.67	at%	Al_2O_3
	O	74.00	at%	
3	Nb	20.67	at%	$Nb_1O_{2.855346}$
	Al	8.12	at%	Al_2O_3
	O	71.20	at%	
4	Nb	18.81	at%	$Nb_1O_{2.935407}$
	Al	10.39	at%	Al_2O_3
	O	70.80	at%	
5	Nb	19.39	at%	$Nb_1O_{2.414647}$
	Al	13.52	at%	Al_2O_3
	O	67.10	at%	
6	Nb	8.93	at%	$Nb_1O_{4.341545}$
	Al	20.93	at%	Al_2O_3
	O	70.15	at%	

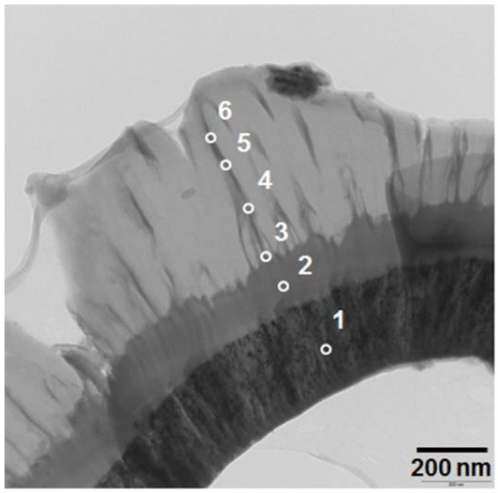

Fig. S4. TEM images of 3 positions of an ultramicrotomed section prepared from an Al/Nb bilayer onto an oxide-coated aluminum foil which had been sequentially anodized/reanodized at 52V/300V. The spots marked on the sections are approximate positions of the electron probes used for EDX analysis. The atomic concentrations of elements in the Al-Nb-O system detected in the 6 spots of each section are given in the relevant tables together with the empirical formulas of niobium oxides in the film material. The Al atoms are supposed to be coordinated with O atoms in aluminum oxide Al_2O_3.

2-D diffractograms and details of interpretation of the XRD results

The background (Chebychev polynomial order 7), sample displacement, cell parameters, crystallite size peak broadening, and the Rietveld scale factor were adjusted in each diffractogram. All the phases possess a remarkable preferred orientation (PO) of the crystallites, as it was firstly deduced from the 2-D diffractograms (Figure S5), where the Debye rings did not show a constant intensity along γ-angle[1].

The crystal structures for each phase detected in the samples are presented in Table S4 together with the results of quantitative analysis of the experimental diffraction patterns. The March-Dollase model[2] was used to correct such preferred orientation in the Rietveld analysis summarized in Table 4. The term PO_{hkl} gives the refined orientation parameter to be applied in a specific [hkl] direction. $PO_{hkl}>1$ means that this direction is not favored while $PO_{hkl}=1$ means

that there is no preferred orientation in this direction. From the table, each phase has a preferred orientation as it can be expected for a thin layer.

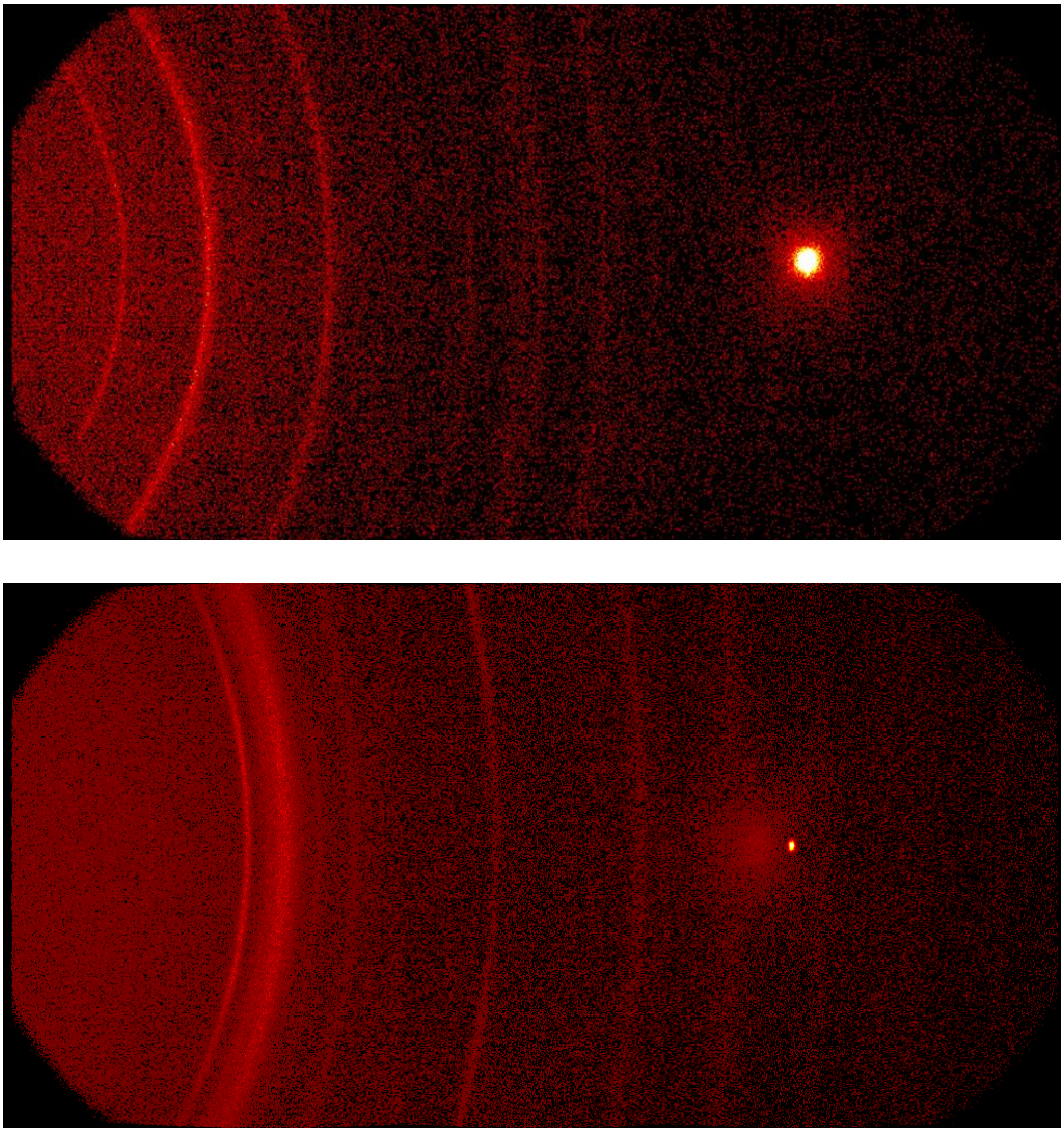

Fig. S5. 2-dimentional diffractograms of (top) the air-annealed alumina-free sample (as in Figure 3f of the paper) and (bottom) the vacuum-annealed alumina-free sample showing the Debye rings of polycrystalline phases and the spots corresponding to the Si single crystal wafers

Table S4. Structural data and refined parameters from the experimental diffractograms: space group, Inorganic Crystal Structure Data file number, cell parameter, mean crystallite size, preferred orientation [hkl] direction with refined correction, and wt% of phases

Phase	Space group	ICSD	Cell (Å)	Crystal. size (nm)	Preferred orientation PO_{hkl}	wt %
			Vacuum-annealed alumina-free sample:			
Nb	Im-3m	076554	a: 3.3882(9)	5.1(2)	[011] 0.25(2)	74.6
NbO	Fm-3m	076560	a: 4.238(1)	14.1(9)	[111] 1.59(4)	15.6
β-NbO_2	$I4_1$	035181	a: 9.670(2)	54(3)	[101] 0.25(4)	6.9
			c: 5.984(1)		[111] 0.33(1)	
Nb_2O_5	Pbam	001840	a: 6.27(1)	63[a)]	[010] 0.71(5)	2.7
			b: 28.66(2)			
			c: 3.939[a)]			
a) these parameters were not refined due to the low intensity of the phase in the diffractogram						
			Air-annealed alumina-free sample:			
Nb_2O_5	Pbam	001840	a: 6.182(2)	26(1)	[010] 0.825(6)	100
			b: 29.248(8)			
			c: 3.939(1)			

Gas-sensor performance analysis

Here we present a comparative analysis of the responses to hydrogen and ethanol gases achieved with the laboratory gas sensor fabricated in the present work with the best responses of niobium-oxide and other metal-oxide gas sensors reported in the literature (references provided)

Table S5. Response time for H_2 detection measured with the nanostructured NO-based laboratory gas sensor fabricated in this work and with the different nanostructured metal-oxide (including niobium oxide)-based sensors found in the literature

Sensing material	Type of nanostructure[a]	H_2 concentration (ppm)	Response time (s)	Ref.
Nb_2O_5[b]	*NCs*	*1000*	*57*	*This paper*
ZnO	NRs	500	resistance is not stabilized after 15 min of gas exposure	[3]
SnO_2	NW	10	100	[4]
ZnO	NR	1000	600	[5]
ZnO	NW	100	~60	[6]
Pt-coated $W_{18}O_{49}$	NW	1000	~60	[7]
Nb_2O_5	NW	2000	127	[8]
Nb_2O_5	NP	10000	90	[9]
Nb_2O_5	NP	1000	300	[10]
Nb_2O_5	thin film	8000	120	[11]

a) NC=nanocolumns, NB= nanobelts, NW= nanowires, NR= nanorods, NP= nanopores

b) Parameters of the material presented in this paper

Table S6. Detection limit for C_2H_5OH measured with the nanostructured NO-based laboratory gas sensor fabricated in the present work and with the different nanostructured metal-oxide (including niobium oxide)-based sensors found in the literature

Sensor Material	Type of nanostructure[a]	Detection limit of C_2H_6O (ppm)	Ref.
Nb_2O_5[b]	*NC*	*2*	*This paper*
V_2O_5	NB	5	[12]
ZnO	NR	10	[13]
In_2O_3	NW	100	[14]
MoO_3	NR	30	[15]
In_2O_5	thin film	10	[16]

a) NC=nanocolumns, NB= nanobelts, NW= nanowires, NR= nanorods, NP= nanopores

b) Parameters of the material presented in the paper

Notes to the porous-anodic-alumina assisted high-potential reanodizing of niobium

With the selected technological, electrical, and electrolytic conditions, in the potential range up to 450 V reanodizing proceeds smoothly, without potential fluctuations (current overshoots), visible gas evolution, stress-generated physical defects, or destructive field crystallization. Moreover, during the potential-stabilization period, the current decreased to its leakage value without dielectric breakdown and unexpected dissolution at the respective interfaces. The sample surface observed in an optical microscope looks defect-free and uniform in color, which is due to interference of light within the anodic film (Figure S6). After selective dissolution of the alumina overlayer, the columnar film observed in an SEM looks uniform across the whole sample surface, without discontinuities or destroyed areas (Figure S7). The length of the columns is essentially the same across the whole sample surface and is determined by the formation potential value only.

Experiments with anodizing of an Al/Nb bilayer sputtered onto a 100-mm Si wafer revealed an extraordinary uniform anodizing behaviour, as well as a good quality of the anodic film across the wafer surface, without local detachment of destruction of the anodized areas (Figure S8).

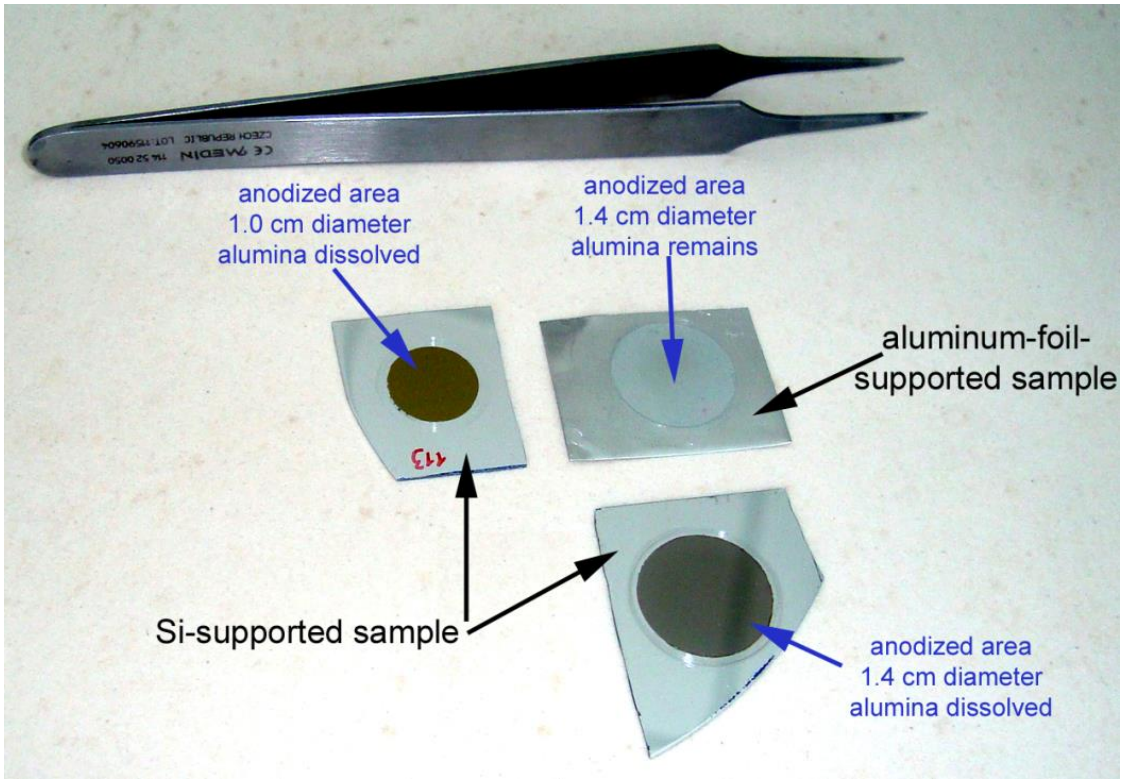

Fig. S6. Digital photo of experimental samples prepared via anodizing an Al/Nb bilayer at 52 V in 0.2 mol dm^{-3} $H_2C_2O_4$ followed by reanodizing in 0.1 mol dm^{-3} H_3PO_4 to 450 V.

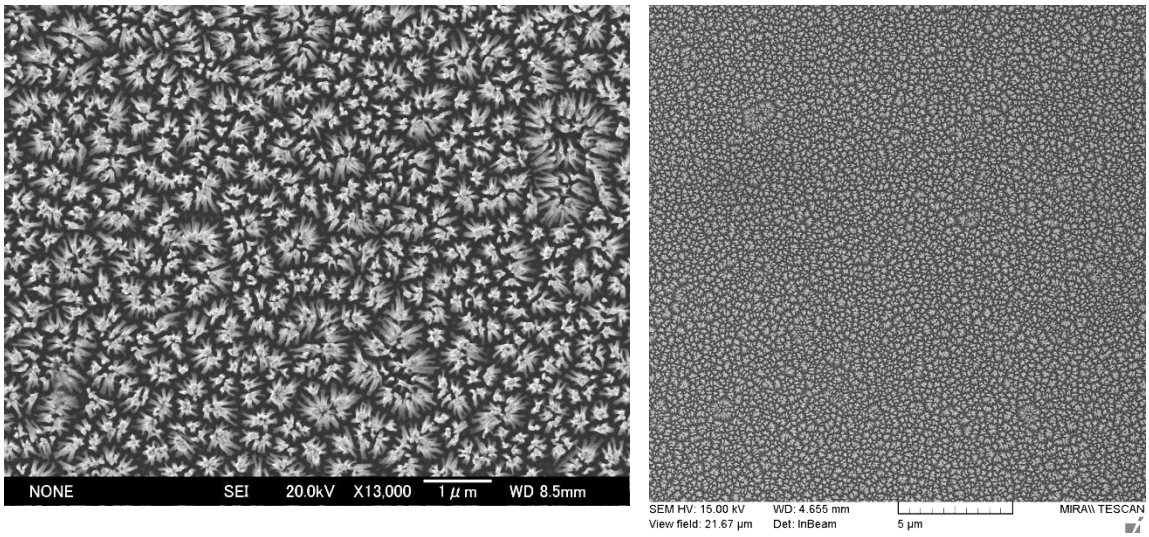

Fig. 7S. Typical SEM surface views of large-surface-area fragments of an Al/Nb bilayer which had been anodized at 52 V in 0.2 mol dm^{-3} $H_2C_2O_4$, reanodized in 0.1 mol dm^{-3} H_3PO_4 to 450 V, and treated in the selective etchant to dissolve the porous alumina overlayer.

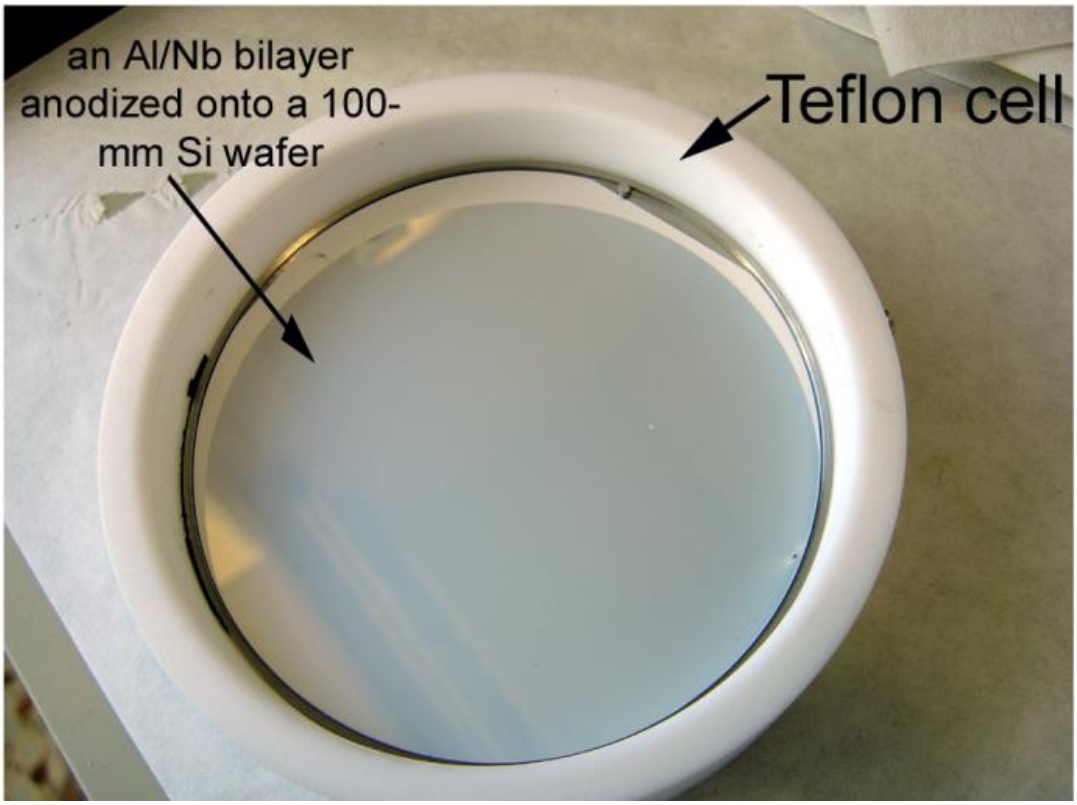

Fig. 8S. Digital photo of an Al/Nb bilayer onto a 100-mm Si wafer anodized/reanodized as mentioned in Figure 7S

REFERENCES

1 B. B. He, in *Two-Dimensional X-ray Diffraction*, A. John Willey & Sons, Inc., Publication 2009, pp 361-390.

2 W. A. Dollase, *J. Appl. Crystallogr*., 1986, **19**, 267-272.

3 H. T. Wang, B. S. Kang, F. Ren, L. C. Tien, P. W. Sadik, D. P. Norton, S. J. Pearton and J. Lin, *Appl. Phys. Lett*., 2005, **86**, 243503-243505.

4 B. Wang, L.F. Zhu, Y. H. Yang, N. S. Xu and G. W. Yang, *J. Phys. Chem. C*, 2008, **112**, 6643-6647.

5 Z. H. Lim, Z. X. Chia, M. Kevin, A. S. W. Wong and G. W. Ho, *Sens. Actuators B*, 2010, **151**, 121-126.

6 R. Khan, H. W. Ra, J. T. Kim, W. S. Jang, D. Sharma and Y. H. Im, *Sens. Actuators B*, 2010, **150**, 389-393.

7 L. F. Zhu, J. C. She, J. Y. Luo, S. Z. Deng, J. Chen, X. W. Ji and N. S. Xu, *Sens. Actuators B*, 2011, **153**, 354-360.

8 Z. Wang, Y. Hu, W. Wang, X. Zhang, B. Wang, H. Tien, Y. Wang, J. Guan and H. Gu, *Int. J. Hydrogen Energy*, 2012, **37**, 4526-4532.

9 R. A. Rani, A. S. Zoolfakar, J. Z. Ou, M. R. Field, M. Austin and K. Kalantar-Zadeh, *Sens. Actuators B*, 2013, **176**, 149-156.

10 T. Hyodo, J. Ohoka, Y. Shimizu and M. Egashira, *Sens. Actuators B*, 2006, **117**, 359-366.

11 T. Hyodo, H. Shibata, Y. Shimizu, M. Egashira, *Sens. Actuators B*, 2009, **142**, 97-104.

12 J. Liu, X. Wang, Q. Peng and Y. Li, *Adv. Mater.*, 2005, **17**, 764- 767.

13 X. Jiaquiang, C. Yuping, L. Yadong and S. Jianian, *J. Mater. Sci.*, 2005, **40**, 2919-2921.

14 C. Xiangfeng, W. Caihong, J. Dongli and Z. Chenmou, *Chem. Phys. Lett.*, 2004, **339**, 461-465.

15 E. Comini, L. Yubao, Y. Brando and G. Sberveglieri, *Sens. Actuators B*, 2005, **407**, 368-371.

16 K. K. Makhija, A. Ray, R. M. Patel, U. B. Trivedi and H. N. Kapse, *Bull. Mater. Sci.*, 2005, **28**, 9-17.